Efficient imaging of crosshole electromagnetic data

Hee Joon Kim[(1)], Ki Ha Lee[(2)], and Mike Wilt[(3)]

[(1)] *Pukyong National University (hejkim@pknu.ac.kr),* [(2)] *Ernest Orland Lawrence Berkeley National Laboratory,* [(3)] *ElectroMagnetic Instruments, Inc.*

ABSTRACT

A computationally efficient inversion scheme has been developed using the extended Born or localized non-linear (LN) approximation to analyze electromagnetic fields obtained in a crosshole environment. The medium is assumed to be cylindrically symmetric about the borehole, and to maintain the symmetry a vertical magnetic dipole is used as a source. The efficiency and robustness of an inversion scheme is very much dependent on the proper use of Lagrange multiplier, which is often provided manually to achieve a desired convergence. We have developed an automatic Lagrange multiplier selection scheme, which enhances the utility of the inversion scheme in handling field data. In this selection scheme, the integral equation (IE) method is quite attractive in speed because Green's functions, the most time consuming part in IE methods, are repeatedly re-usable throughout the selection procedure. The inversion scheme using the LN approximation has been tested to show its stability and efficiency using synthetic and field data.

KEY WORDS: crosshole, localized nonlinear approximation, cylindrical symmetry, inversion

INTRODUCTION

High-resolution imaging of electrical conductivity has been the subject of many studies in crosshole tomography using electromagnetic (EM) fields (Zhou et al., 1993; Wilt et al., 1995; Alumbaugh and Morrison, 1995; Newman, 1995; Alumbaugh and Newman, 1997). Although the theoretical understanding and associated field practices for crosshole EM methods are relatively mature, fast and stable interpretation of crosshole EM data is still a challenging problem.

The main advantage of integral equation (IE) method in comparison with the finite difference (FD) and/or finite element (FE) method is the fast and accurate simulation of compact three-dimensional (3-D) bodies in a layered background (Hohmann, 1975). The FD and FE methods are suitable for modeling EM fields in complex structures with large-scale conductivity variations. In principle, the IE method can handle these models too, but the huge demand on computer resources places a practical limit on its use. This is because of the full matrix arising from the IE formulation.

Another advantage of the IE method over the FD or FE method is its greater suitability for inversion. The IE formulation readily contains a sensitivity matrix, which can be revised at each inversion iteration at little expense. With the FD or FE method, in contrast, the sensitivity matrix has to be recomputed at each iteration at a cost nearly equal to that of full forward modeling. The IE method, however, has to overcome severe practical limitations imposed on the numerical size of the anomalous domain for inversion purposes. In this direction, several approximate methods such as the localized nonlinear (LN) approximation (Habashy et al., 1993) and quasi-linear approximation (Zhdanov and Fang, 1996) have been developed recently.

In this paper we exploit an advantage of the LN approximation with applications to crosshole inversion of EM data. We begin our discussion with a review of the LN approximation of IE solutions. We then consider its accuracy for a cylindrically symmetric model, describe our inversion algorithm, and demonstrate the stability and effectiveness of this approach by inverting synthetic data. Finally, we briefly consider an example application to field data provided by Chevron as a part of the Lost Hills CO_2 pilot project in southern California.

LN APPROXIMATION

Assuming an $e^{+i\omega t}$ time dependency and an electric current source $\mathbf{J}_s$ at $\mathbf{r}_s$, Maxwell's equations in the frequency domain are (Hohmann, 1975)

$$\nabla \times \mathbf{E}(\mathbf{r}) = -i\omega\mu\mathbf{H}(\mathbf{r}) , \tag{1}$$

$$\nabla \times \mathbf{H}(\mathbf{r}) = \sigma(\mathbf{r})\mathbf{E}(\mathbf{r}) + \mathbf{J}_s(\mathbf{r} - \mathbf{r}_s) , \tag{2}$$

where $\mathbf{E}$ and $\mathbf{H}$ are the electric and magnetic fields, respectively, σ the conductivity, and ω the angular frequency, and μ the magnetic permeability. For the frequency range used in this study (less than 100 kHz), the displacement current can be neglected, and the magnetic permeability μ is assumed to be that of free space. The electrical conductivity σ is heterogeneous and can be divided into

$$\sigma(\mathbf{r}) = \sigma_b + \Delta\sigma(\mathbf{r}) , \tag{3}$$

where σ_b is the background conductivity, and $\Delta\sigma$ is the excess conductivity. From equations (1) and (2), we can get a differential equation for the electric field as

$$\nabla \times \nabla \times \mathbf{E}(\mathbf{r}) + i\omega\mu\sigma(\mathbf{r})\mathbf{E}(\mathbf{r}) = -i\omega\mu\mathbf{J}_s(\mathbf{r}) . \tag{4}$$

The numerical solution for the electric field may be obtained using either the FE or FD method. Alternatively, the numerical solution may be obtained using the IE method involving the Green's function that satisfies

$$\nabla\times\nabla\times\mathbf{G}_E(\mathbf{r}-\mathbf{r}')+i\omega\mu\sigma_b\mathbf{G}_E(\mathbf{r}-\mathbf{r}')=\mathbf{I}\delta(\mathbf{r}'-\mathbf{r}_s)\,, \quad (5)$$

where **I** is the identify tensor, and the subscript *E* signifies that the Green's function translates current source **J** to electric field **E**. Each vector component of the Green's tensor $\mathbf{G}_E(\mathbf{r}\text{-}\mathbf{r}')$ is the vector electric field at **r** due to a point source at **r′** with its current density of $-(i\omega\mu)^{-1}$ Amp/m^2, polarized in *x*, *y*, and *z*, respectively. Using equations (4) and (5), we can derive an IE solution for the electric field as

$$\mathbf{E}(\mathbf{r})=\mathbf{E}_b(\mathbf{r})-i\omega\mu\int_V\mathbf{G}_E(\mathbf{r}-\mathbf{r}')\cdot\Delta\sigma(\mathbf{r}')\mathbf{E}(\mathbf{r}')dv'\,, \quad (6)$$

where $\mathbf{E}_b(\mathbf{r})$ is the background electric field that would exist in the presence of background medium only, and the term $\Delta\sigma\mathbf{E}$ inside the integral is called the scattering current (Hohmann, 1975).

Equation (6) is nonlinear because the electric field inside the integral is a function of the conductivity. To obtain a numerical solution, the anomalous body is divided into a number of cells, and a constant electric field is assigned to each cell. Since Raiche (1974) first formulated a volume 3-D IE method, many numerical solutions have been presented on this subject (Hohmann, 1988). The process involved in volume IE methods requires computing time proportional to the number of cells used, and it quickly becomes impractical as the size of the inhomogeneity is increased to handle realistic problems.

For some important class of problems the complexity associated with a full 3-D problem can be reduced to something much simpler. A model whose electrical conductivities are cylindrically symmetric in the vicinity of a borehole is such an example. In order to preserve the cylindrical symmetry in the resulting EM fields, a horizontal loop current source or a vertical magnetic dipole may be considered in the borehole. In this case the problem is scalar when formulated using the azimuthal electric field E_φ, and the analogous IE solution is

$$E_\varphi(\mathbf{r})=E_{\varphi b}(\mathbf{r})-2\pi i\omega\mu\iint_{\rho\,z}G_E(\mathbf{r}-\mathbf{r}')\Delta\sigma(\mathbf{r}')E_\varphi(\mathbf{r}')\rho'd\rho'dz'\,, \quad (7)$$

where

$$\mathbf{r}=\vec{\rho}+\vec{z}\quad\text{and}\quad\mathbf{r}'=\vec{\rho}'+\vec{z}'$$

are the position vectors, and the electric field and Green's function are both scalar. The Green's function is given in the form of a Hankel transform as (p. 219, Ward and Hohmann, 1988)

$$G_E(\mathbf{r}-\mathbf{r}')=-\frac{1}{4\pi}\int_0^\infty\frac{e^{-u_b|z-z'|}}{u_b}\lambda J_1(\lambda\rho)J_1(\lambda\rho')d\lambda\,, \quad (8)$$

where

$$u_b=(\lambda^2+i\omega\mu\sigma_b)^{1/2}.$$

Since measurements are usually made for the magnetic field, equation (7) is modified as

$$H_z(\mathbf{r})=H_{zb}(\mathbf{r})-2\pi i\omega\mu\iint_{\rho\,z}G_H(\mathbf{r}-\mathbf{r}')\Delta\sigma(\mathbf{r}')E_\varphi(\mathbf{r}')\rho'd\rho'dz'\,, \quad (9)$$

where $\mathbf{G}_H(\mathbf{r}\text{-}\mathbf{r}')$ translates the scattering current $\Delta\sigma(\mathbf{r}')E_\varphi(\mathbf{r}')$ at **r**' to the magnetic field at **r**.

Using equations (7) through (9), we can obtain an IE solution by first dividing the (ρ, *z*) cross-section into a number of cells, and formulate a system of equations for the electric field using a pulse basis function. Sena and Toksoz (1990) presented a crosshole inversion study for permittivity and conductivity in cylindrically symmetric medium using high-frequency EM, and Alumbaugh and Morrison (1995) investigated crosshole EM tomography using an iterative Born approximation.

The LN approximation offers an efficient and reasonably accurate electric field solution without deriving the full IE solution from equation (7). To do this equation (7) is first modified to (Habashy et al., 1993)

$$E_\varphi(\mathbf{r})+2\pi i\omega\mu E_\varphi(\mathbf{r})\iint_{\rho\,z}G_E(\mathbf{r}-\mathbf{r}')\Delta\sigma(\mathbf{r}')\rho'd\rho'dz'=E_{\varphi b}(\mathbf{r})-2\pi i\omega\mu\iint_{\rho\,z}G_E(\mathbf{r}-\mathbf{r}')\Delta\sigma(\mathbf{r}')\left[E_\varphi(\mathbf{r}')-E_\varphi(\mathbf{r})\right]\rho'd\rho'dz'$$

If the electric field is continuous in the vicinity of **r**, the contribution from the second integral may be small compared with the background electric field. This is because when **r′** approaches **r**, the difference in $[E_\varphi(\mathbf{r}')-E_\varphi(\mathbf{r})]$ is getting smaller, so the scattering current is effectively zero at the singular point. When **r′** moves away from **r,** the contribution is also small because the Green's function falls off rapidly. For the type of problem where there is only the azimuthal electric field, therefore, we can get a good approximation even if the second integral is neglected entirely. As a result we get

$$E_\varphi(\mathbf{r})\approx\gamma(\mathbf{r})E_{\varphi b}(\mathbf{r})\,, \quad (10)$$

where

$$\gamma(\mathbf{r})=\left[1+2\pi i\omega\mu\iint_{\rho\,z}G_E(\mathbf{r}-\mathbf{r}')\Delta\sigma(\mathbf{r}')\rho'd\rho'dz'\right]^{-1}.$$

Substituting equation (10) into equation (9), we get an approximate magnetic field solution

$$H_z(\mathbf{r})\approx H_{zb}(\mathbf{r})-2\pi i\omega\mu\iint_{\rho\,z}G_H(\mathbf{r}-\mathbf{r}')\Delta\sigma(\mathbf{r}')\gamma(\mathbf{r}')E_{\varphi b}(\mathbf{r}')\rho'd\rho'dz'\,. \quad (11)$$

To illustrate the efficiency and usefulness of the LN numerical solution, especially in a crosshole application, let us consider a simple model consisting of a conductive ring about a source borehole axis in a uniform whole space of 100 ohm-m. The cross-section of the ring is a 10 m by 10 m rectangle and 15 m horizontally away from the borehole as shown in Figure 1. The Born and LN approximated magnetic fields measured in the other borehole 50 m horizontally away from the source borehole are compared with the result obtained from the full FE method (Lee et al., 2002).

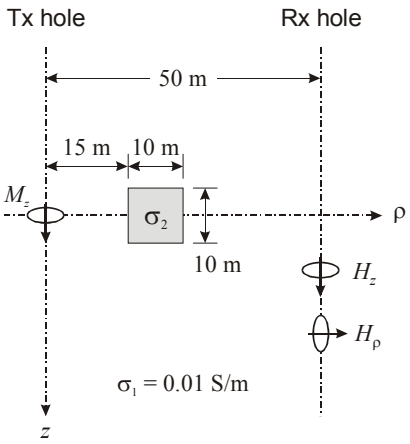

Figure 1. A cylindrically symmetric model. A conductive body with a cross-section of 10 m by 10 m is cylindrically symmetric about a borehole in which vertical magnetic dipole (M_z) source is inserted, and located in a whole space of 0.01 S/m at 15 m horizontally away from the borehole. Horizontal and vertical magnetic fields are measured in the other borehole 50 m horizontally away from the source borehole.

Figure 2 shows the comparison in the secondary horizontal and vertical magnetic fields between the Born, LN, and FE solutions. The center of the body is chosen as z = 0. The conductivity contrast and operating frequency used are 10 and 10 kHz, respectively. The source and receiver are located at the same depth in each borehole. More anomalies can be observed in the imaginary part than in the real part. For all field components, the LN and FE solutions agree very well.

We are also interested in the quality of the LN solution when the conductivity of the body is varied. Figure 3 shows the comparison in the secondary vertical magnetic fields between the Born, LN, and FE solutions. A vertical magnetic source is fixed at the depth of the center of body in the source borehole, and vertical magnetic fields are measured at 10 m below the center of the body in the receiver borehole. The frequency used is 10 kHz. The LN approximation is very well up to the conductivity contrast of about 100. The imaginary part of the LN solution starts deviating from the FE solution beyond the conductivity contrast of 100, while the real part still shows a good agreement.

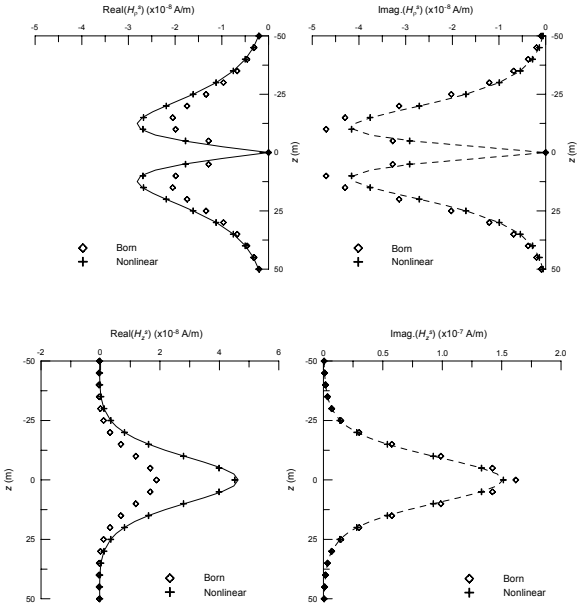

Figure 2. Horizontal (upper) and vertical (lower) components of secondary magnetic fields. Operating frequency is 10^4 Hz and body conductivity is 0.1 S/m. The array used is a crosshole source-receiver pair moving in parallel down the two boreholes. Solid and dashed lines show FE solutions.

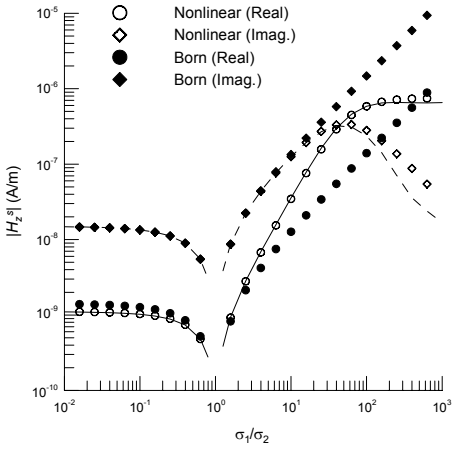

Figure 3. The effect of conductivity contrast between the body and background on the vertical components of secondary magnetic fields. The depths of source and receiver are fixed at 5 m above and below the bottom of the body, respectively. The operating frequency is 10^4 Hz. Solid and dashed lines show FE solutions.

Finally, the comparison is made for responses in frequency as shown in Figure 4. The source-receiver array is the same as that in Figure 3, and the conductivity contrast is fixed to 10. The LN and FE solutions show a good agreement all the way up to about 100 kHz.

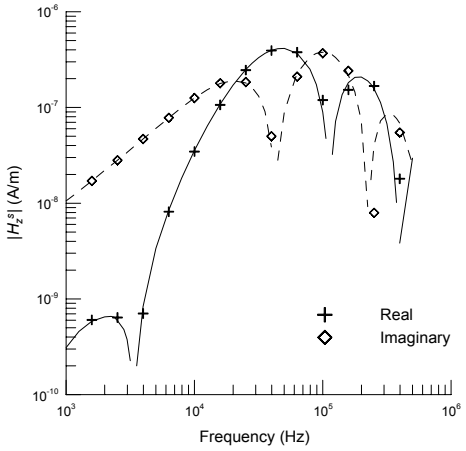

Figure 4. The effect of frequency on the vertical components of secondary magnetic fields. The depths of source and receiver are fixed at 5 m above and below the bottom of the body, respectively. The conductivity of the body is 0.1 S/m. Solid and dashed lines show FE solutions.

INVERSION

Based on the encouraging results of the LN approximation, we have proceeded to implement the crosshole EM inversion. Measurements are in the other borehole to the transmitter borehole. Upon dividing the inhomogeneity into K elements, the secondary magnetic field at the i-th receiver in the borehole may be written as

$$H_{zi}^s \approx -2\pi i\omega\mu \sum_{k=1}^{K} \Delta\sigma_k \gamma_k E_{\varphi bk} \iint_{S_k} G_H(\rho', z_i - z')\rho' d\rho' dz', \tag{12}$$

where the subscript k denotes the k-th element. The corresponding Green's function for the magnetic field may be deduced from the electric field Green's function (8) as

$$G_H(\rho, z_i - z') = \frac{1}{4\pi i\omega\mu} \int_0^\infty \frac{e^{-u_b|z-z'|}}{u_b} \lambda^2 J_1(\lambda\rho')d\lambda \,. \tag{13}$$

For the inversion, the sensitivity of the magnetic field with respect to the change in conductivity can be easily obtained from equation (12). Taking derivative of the data with respect to the j-th conductivity parameter and neglecting the dependence of γ_j on $\Delta\sigma_j$, the sensitivity becomes

$$\frac{\partial H_{zi}^s}{\partial \sigma_j} \approx -2\pi i\omega\mu\gamma_j E_{\varphi bj} \iint_{S_j} G_H(\rho', z_i - z')\rho' d\rho' dz', \tag{14}$$

which can be easily evaluated by integrating over the j-th element.

The inversion procedure starts with the data misfit $\|\mathbf{W}_d[\mathbf{H}(\sigma)-\mathbf{H}_d]\|^2$, where the subscript d denotes data. The data weighting matrix $\mathbf{W}_d$ is used to give relative weights to individual data. If a perturbation $\delta\sigma$ is allowed to the conductivity, the misfit takes a form $\|\mathbf{W}_d[\mathbf{H}(\sigma+\delta\sigma)-\mathbf{H}_d]\|^2$, and the total objective functional may be written as

$$\phi = \left\|\mathbf{W}_d[\mathbf{H}(\sigma + \delta\sigma) - \mathbf{H}_d]\right\|^2 + \lambda\left\|\mathbf{W}_\sigma \delta\sigma\right\|^2, \tag{15}$$

where the second term on the right-hand side is added to impose a smoothness constraint, and $\mathbf{W}_\sigma$ is the weighting matrix and λ is the Lagrange multiplier that controls the trade-off between data misfit and parameter smoothness. Expanding the misfit in $\delta\sigma$ using the Taylor series, discarding terms higher than the square term, and letting the variation of the functional with respect to $\delta\sigma$ equal to zero, we obtain a linear system of equations for the perturbation $\delta\sigma$ as

$$(\mathbf{J}^T\mathbf{W}_d^T\mathbf{W}_d\mathbf{J} + \lambda\mathbf{W}_\sigma^T\mathbf{W}_\sigma)\delta\sigma = -\mathbf{J}^T\mathbf{W}_d^T\mathbf{W}_d[\mathbf{H}(\sigma) - \mathbf{H}_d], \tag{16}$$

where the superscript T indicates the matrix transpose, and the entries of Jacobian matrix $\mathbf{J}$ are the sensitivity functions given in equation (14).

The stability of the inversion is largely controlled by requiring the conductivity to vary smoothly. Larger values of λ result in smooth and stable solutions at the expense of resolution. It even allows for the solution of grossly underdetermined problems (Tikhonov and Arsenin, 1977). In this crosshole inversion study, the parameter λ is progressively selected in the inversion process. The selection procedure starts with executing a given number of inversions using $n\ell$ different multipliers that are spaced appropriately. The same Jacobian is used at this step. As a result $n\ell$ updated parameter sets are produced, followed by $n\ell$ forward model calculations resulting in $n\ell$ data misfits. Among these, we choose the model and parameter λ giving the lowest data misfit as optimum ones. In this selection scheme, the IE modeling is quite attractive in speed because Green's functions, the most time consuming part in IE methods, are repeatedly re-usable throughout the selection procedure.

To evaluate the performance of extended Born inversion using the LN approximation, we choose a

conductivity model shown in Figure 5. The model consists of two cylindrically symmetric bodies, one conductive (0.1 S/m) and the other resistive (0.001 S/m), in a whole space of 0.01 S/m. A FE scheme (Lee et al., 2002) is used to generate synthetic data. The accuracy of the FE method is estimated as a level of less than 1 %. Using a vertical magnetic dipole (M_z) as a source, vertical magnetic fields (H_z) are computed at three frequencies of 2.5 kHz, 10 kHz and 20 kHz. Three-percent Gaussian noise is added to the synthetic data prior to the inversion. The inversion is started with an initial model of 60 ohm-m uniform whole space. In this test $n\ell = 3$ is used in each iteration to select parameter update and Lagrange multiplier.

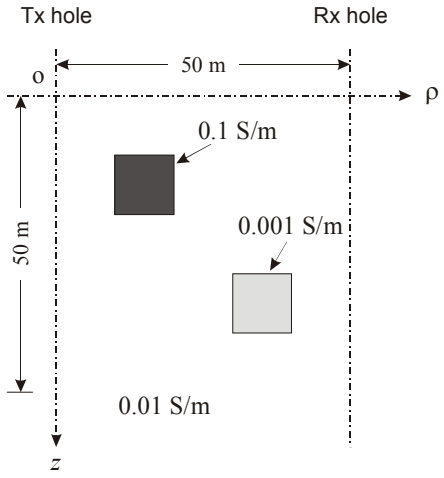

Figure 5. A model used to calculate synthetic data for inversion test. Two bodies of 0.1 S/m and 0.001 S/m, separated vertically by 10 m, are located in a whole-space of 0.01 S/m. The upper conductive and lower resistive ones are at 10 m and 30 m horizontally away from the source borehole, respectively.

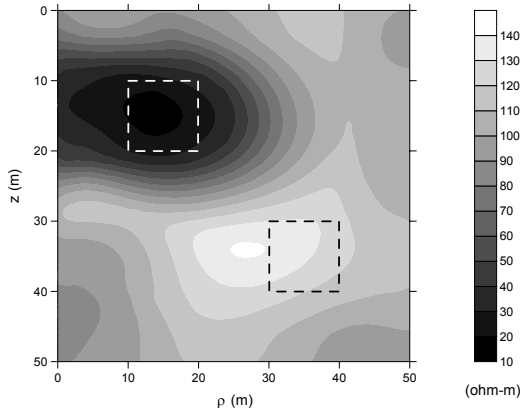

Figure 6. An image of the two conductors reconstructed from the inversion of synthetic data after 8th iteration.

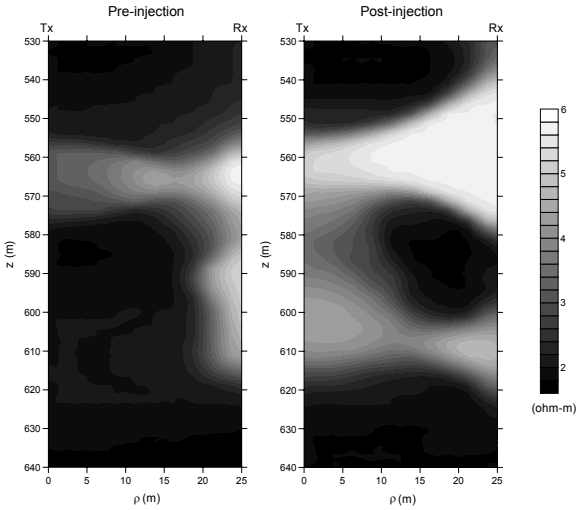

Figure 7. Resistivity imaging derived from the 2-D inversion of data obtained in the Lost Hills CO_2 pilot project in southern California.

After 8 iterations, the two bodies are clearly reconstructed as shown in Figure 6. The recovered conductivity is found to be nearly the same in the conductive body but is overestimated in the resistive body. The inversion process is quite stable, and the rms misfit decreases from the initial guess of 5.095 to 0.036 after 8 iterations. The smoothing parameter varies significantly during the inversion process. This means it is difficult to determine the parameter a priori.

Finally, the 2-D inversion algorithm has been applied to a set of crosshole field data provided by Chevron as a part of the Lost Hills CO_2 pilot project in southern California (Wilt, 2002). The separation between the two vertical boreholes is 24.536 m and CO_2 injection well is near the center of the section defined by the two wells. Although both EM and seismic data for the pre- and post-injection are available, we conducted inversion using only the EM (M_z-H_z) data. The operating frequency was 759 Hz.

Figure 7 shows inversion results of the crosshole data. The CO_2 injection into a reservoir of oil/brine mixture results in changes in conductivity, which can be indirectly interpreted as the displacement of brine with injected CO_2. The replacement of water with CO_2 makes a decrease of conductivity. Figure 7 shows a significant change in conductivity distribution, and this increase of resistivity suggests an effect of the CO_2 injection. Unfortunately, the borehole separation is not far enough compared with the skin depth (i.e., low frequency), the reconstructed images using the assumption of cylindrically symmetric may have artifacts that can be produced by the geometry of conductive zone outside of the interwell plane (Alumbaugh and Morrison, 1995). Computing time required for the 2-D approximate inversion is less than 5 minutes on a Pentium-4 PC to

obtain 650 conductivities from 604 complex H_z fields after 5 iterations.

CONCLUSIONS

The extended Born or LN approximation of IE solution has been applied to inverting crosshole EM data using a cylindrically symmetric model. The extended Born approximation is less accurate than a full solution but much superior to the simple Born approximation. When applied to the cylindrically symmetric model with a vertical magnetic dipole source, however, the extended Born approximation works well because electric fields are scalar and continuous everywhere. One of the most important steps in the inversion is the selection of a proper regularization parameter for stability. The LN solution provides an efficient means for selecting an optimum regularization parameter, because Green's functions, the most time consuming part in IE methods, are repeatedly re-usable at each iteration. In addition, the IE formulation readily contains a sensitivity matrix, which can be revised at each iteration at little expense. The inversion scheme using the LN approximation developed in this study has been tested on its stability and efficiency using synthetic and field data.

ACKNOWLEDGEMENTS

This work was supported by the Assistant Secretary for Energy Efficiency and Renewable Energy, Office of Wind and Geothermal Technologies of the U.S. Department of Energy under Contract No. DE-AC03-76SF00098. We would like to thank Michael Morea, Chevron USA Production Company, and the US Department of Energy, National Petroleum Technology Office, (Class III Field Demonstration Project DE-FC22-95BC14938) for allowing us to publish this data. Korea Science and Engineering Foundation (R01-2001-000071-0) provided support for this study.

REFERENCES

Alumbaugh, D. L. and Morrison, H.F., 1995, Theoretical and practical considerations for crosswell electromagnetic tomography assuming a cylindrical geometry, *Geophysics*, **60**, 846-870.

Alumbaugh, D. L., and Newman, G. A., 1997, Three-dimensional massively parallel electromagnetic inversion—II. Analysis of crosswell electromagnetic experiment, *Geophys. J. Int*., **128**, 355-363.

Habashy, T. M., Groom, R. M., and Spies, B. R., 1993, Beyond the Born and Rytov approximations: a nonlinear approach to electromagnetic scattering, *J. Geophys. Res*., **98**, 1795-1775.

Hohmann, G. W., 1975, Three-dimensional induced polarization and EM modeling, *Geophysics*, **40**, 309-324.

Hohmann, G. W., 1988, Numerical modeling for electromagnetic methods of geophysics, *in* Nabighian, M.N., Ed., Electromagnetic methods in applied geophysics, Vol. 1, Soc. Expl. Geophys., 313-363.

Lee, K. H., Kim, H. J., and Uchida, T., 2002, Electromagnetic fields in steel-cased borehole, *Geophys. Prosp*. (submitted)

Newman, G. A., 1995, Crosswell electromagnetic inversion using integral and differential equations, *Geophysics*, **60**, 899-911.

Raiche, A. P., 1974, An integral equation approach to 3D modeling, *Geophys. J. Roy. Astr. Soc.,* **36**, 363-376.

Sena, A. G., and Toksoz, M. N., 1990, Simultaneous reconstruction of permittivity and conductivity for crosshole geometries, *Geophysics*, **55**, 1302-1311.

Tikhonov, A. N., and Arsenin, V. Y., 1977, Solutions to Ill-Posed Problems, John Wiley and Sons, Inc.

Ward, S. H., and Hohmann, G.W., 1988, Electromagnetic Theory for Geophysical Applications, *in* Nabighian, M.N., Ed., Electromagnetic methods in applied geophysics, Investigations in Geophysics 3, Vol. 1: Soc. Expl. Geophys.

Wilt, M. J., Alumbaugh, D. L., Morrison, H. F., Becker, A., Lee, K. H., and Deszcz-Pan, M., 1995, Crosshole electromagnetic tomography: System design considerations and field results: *Geophysics*, **60**, 871-885.

Wilt, M. J., Mallan, R., Kasameyer, P., and Kirkendall, B., 2002, 3D extended logging for geothermal resources: Field trials with the Geo-BILT system, Proc. 27th Workshop on Geothermal Reservoir Engineering, Stanford Univ., SGP-TR-171.

Zhdanov, M. S., and Fang, S., 1996, Quasi-linear approximation in 3-D EM modeling, *Geophysics*, **61**, 646-665.

Zhou, Q., Becker, A., and Morrison, H. F., 1993, Audio-frequency electromagnetic tomography in 2-D, *Geophysics*, **58**, 482-495.